CZECH TECHNICAL UNIVERSITY IN PRAGUE

FACULTY OF MECHANICAL ENGINEERING

Department of Process Engineering

Bachelor Thesis

2020 Ahsanulnas Miardi

CZECH TECHNICAL UNIVERSITY IN PRAGUE

FACULTY OF MECHANICAL ENGINEERING
Department of Process Engineering

Experimental and CFD analysis of feed pellets in fish tank

Bachelor Thesis

Study program: Bachelor of Mechanical Engineering

Study branch: Mechanical Engineering

Supervisor: doc .Ing. Karel Petera, Ph.D.

Ahsanulnas Miardi

Prague, January 2020

BACHELOR'S THESIS ASSIGNMENT

I. Personal and study details

Student's name: **Miardi Ahsanulnas** Personal ID number: **441694**

Faculty / Institute: **Faculty of Mechanical Engineering**

Department / Institute: **Department of Process Engineering**

Study program: **Bachelor of Mechanical Engineering**

Branch of study: **Power and Process Technology**

II. Bachelor's thesis details

Bachelor's thesis title in English:

Experimental and CFD analysis of feed pellets in fish tank

Bachelor's thesis title in Czech:

Experimental and CFD analysis of feed pellets in fish tank

Guidelines:

- Make a literature research concerning CFD methods useful for description of moving particles in fluid
- Try to perform experiments identifying basic properties of fish feed pellets necessary for CFD analysis
- Perform CFD simulations of feed pellets in a fish tank of given geometry
- Summarize the results and propose possible improvements in future work

Bibliography / sources:

According to the recommendation of the thesis supervisor.

Name and workplace of bachelor's thesis supervisor:

doc. Ing. Karel Petera, Ph.D., Department of Process Engineering, FME

Name and workplace of second bachelor's thesis supervisor or consultant:

Date of bachelor's thesis assignment: **31.10.2019** Deadline for bachelor thesis submission: **10.01.2020**

Assignment valid until: _____

doc. Ing. Karel Petera, Ph.D.	prof. Ing. Tomáš Jirout, Ph.D.	prof. Ing. Michael Valášek, DrSc.
Supervisor's signature	Head of department's signature	Dean's signature

III. Assignment receipt

The student acknowledges that the bachelor's thesis is an individual work. The student must produce his thesis without the assistance of others, with the exception of provided consultations. Within the bachelor's thesis, the author must state the names of consultants and include a list of references.

31/10/2019

Date of assignment receipt

Student's signature

Declaration

I hereby declare that I have completed this thesis entitled **Experimental and CFD analysis of feed pellets in fish tank** independently with consultations with my supervisor and I have attached a full list of used references and citations.

I do not have a compelling reason against the use of the thesis within the meaning of Section 60 of the Act No.121/2000 Coll., on copyright, rights related to copyright and amending some laws (Copyright Act).

In ...Prague..., Date: .....

……

Student Signature

ACKNOWLEDGEMENT

I would like to express my sincere gratitude and respect towards my thesis supervisor, Dr. Karel Petera. The continuous support and guidance with him were of great help for the successful completion of the work and I learned a lot from him.

Finally, I would like to express my love and affection towards my mother whom I owe so much that can never be repaid and my friends for the unwavering support throughout my life and studies.

ABSTRACT

The present work was carried out to investigate particle behavior in the conical fish tank provided by Lika et al., (2015) using the CFD-DPM approach. CFD (Computational Fluid Dynamics) analysis was performed to obtain developed flow field around the tank based on $k-\omega$ SST (Shear-Stress-Transport) turbulence model. A sedimentation experiment was carried out to determine properties of the pellets. A simple one-way coupling model was performed in order to evaluate the particle motion. From DPM (discrete phase model) simulation, it was found that particle with a density slightly higher than water (approximately 1000 kg/m^3) will settle less than a minute compared to a particle having the same density as the water in 500l tank. The methodology used in this work could help aquaculturits and other researchers to determine optimal properties of feed pellets.

Keywords: Conical fish tank, Sedimentation, $k-\omega$ SST, CFD-DPM, One-way coupling

CONTENTS

Chapters	Title	Page No.
	LIST OF FIGURES	vii
	LIST OT TABLES	viii
Chapter-I	**Introduction**	
1.1	Terminal velocity and drag coefficient of particle	2
	1.1.1 Particle Movement Through Fluid due to Gravitational Field	2
	1.1.2 Stationary Particle Movement – Free Settling	3
	1.1.3 Drag on Non-Spherical Particle	4
1.2	Experimental Methods for the Measurement of Particle Drag Coefficient	5
1.3	Particle Size Characterization	6
1.4	Objective of this work	6
Chapter-II	**CFD-DPM**	
2.1	CFD Software Packages	8
	2.1.1 Preprocessor	8
	2.1.2 Solver	9
	2.1.2 Post processing	9
2.2	Principle of computational fluid dynamics	9
	2.2.1 Introduction to governing equation	9
	2.2.2 The continuity equations	9
	2.2.3 The momentum equations	10
	2.2.4 The energy equations	11
	2.2.5 Comment on the governing equations	11
	2.2.6 Turbulent modelling	12
2.3	Principle of discrete phase model	13
	2.3.1 Eulerian verses Lagrangian model	13
	2.3.2 Modelling discrete phase	13
	2.3.3 Simplified assumptions of discrete phase model	14
	2.3.4 Particle force balance	14
	2.3.5 Definition of coupling between phases	15
Chapter-III	**Experiment and Result**	
3.1	Sample	16
3.2	Vertical column set up	16
3.3	Result	
	3.1.1 Obtaining density based on settling velocity	17
3.4	Discussion	20

Chapter-IV	**CFD-DPM Modelling**	
4.1	Numerical method and model descriptions	21
	4.1.1 Introduction	21
	4.1.2 Tank Geometry	22
	4.1.3 Computational mesh and the quality	22
	4.1.4 Grid convergence index	25
	4.1.5 Turbulent modelling based on RANS	26
	4.1.6 Realizable $k-\varepsilon$ model	27
4.2	Setting initial conditions for the discrete phase modelling	27
	4.2.1 Injection type	27
	4.2.2 Material	28
	4.2.3 Coupling	28
Chapter-V	**CFD-DPM Simulation**	
5.1	CFD problem setup	30
	5.1.1 Solver	30
	4.2.2 Boundary conditions	30
5.2	Results and comparison of magnitude velocity	30
5.3	Particle motion	32
Chapter-VI	**Conclusions**	34
	Reference	36

LIST OF FIGURES

Figure No.	Description	Page No.
1	Forces acting on particle as it settle down fluid medium	2
2	Sample pellet TM0 – The red box is an outline parameter of the sample measured against real scale	17
3	Setup sketch to illustrate feed pellet settling in water column (tap water was used). This experiment was used to determine settling velocity and effective density of the feed particle.	17
4	500l Tank Geometry – unit in cm (Lika & M. M. Pavlidis, 2015)	21
5	Geometrical Model of Fish Tank by Design Modeler ANSYS Fluent	22
6	Skewness and orthogonal quality mesh metrics spectrums.	23
7	Meshing of Modelled Geometry	24
8	Illustration of polyhedral mesh of the fish tank used in CFD simulation. Total number of mesh elements after the polyhedral conversion was 258 000	25
9	Contour of vertical velocity components in three horizontal planes in the fish tank at different inlet velocity operating parameter in m/s.	30
10	Feed pellet dispersion in fish tank injected from free surface.	31
11	1 Fish pellet TM0 injected from surface with the same effective density as fluid (water) at different water inlet parameter	32
12	Contour of vertical velocity components with k-ω SST turbulence model	33

LIST OF TABLES

Table No.	Description	Page No.
1	Sample of test pellets provided by University of South Bohemia, FFPW.	16
2	Experimental result of TM0 from batch 1	18
3	Experimental result of TM75 from batch 1	18
4	TM0 after soaking for 15 minutes and new settling velocity	19
5	TM75 after soaking for 15 minutes and new settling velocity	19
6	Example of mesh quality measures for the generated grid (mesh) according to Ipek (2019).	24
7	Quality of two different mesh depending on their type of meshing	27
8	Parameter condition for Discrete Phase Module (DPM)	28

CHAPTER I INTRODUCTION

With an anticipated 10 billion people expected to inhabit the planet by 2050, the animal protein demand keeps rising, while the production of capture fish has been stagnant for the past two decades. By the year 2030, 62 percent of all seafood production will come from aquaculture. Given that overfishing of our oceans and other natural resources is continuously increasing year over year, humans need alternate sources for seafood to feed the planet's ever-growing. This makes aquaculture to become one of the fastest-growing food industry in the world (Alliance Global Aquaculture (Alliance, 2019).

Fish feeding is one of the most important factors in commercial fish farming because feeding regime may have consequences on both growth performance and feed wastage (Tsevis, 1992). A problem arises when undigested feed pellets and do not naturally leave the tank through an outlet and accumalated in the tank for a long period of time. An impact on fish welfare can be devastating. This is due mainly to the low quality of water that will increase the stress on the culture of organism (Rosenthal, 1982; Braaten, 1986).

The size of fish pellet and the rate which they are delivered may affect the amount of feed that an individual fish can ingest over a period of time. Sub-optimal size pellets or high amount of pellets may cause feed wastage, as fish may be unable to catch large numbers of pellets before they sink through (Tvinnereim, 1988).

Fish welfare and production rate are also influenced by the tank hydrodynamics i.e. their designation must follow speciation while maintaining uniformity of rearing condition, fast elimination of waste and uniform distribution of fish throughout the tank (Tvinnereim, 1988). Influence of velocity in which tank should adopt the certain level of turbulence must be acknowledged to avoid loss of fish muscle tone and the respiration system (Tvinnereim, 1988). Models of these features conditions have been well established by many authors over the last few decades.

Although it is crucial to implement such construction either adjusting inlet which was largely dependent on the overall flow pattern (Muller, et al,. 2017), or experiments on different geometry of the tank itself, we could also look at another approach which describe the behavior of pellet settling inside the tank during feeding activity.

The main parameter controlling the sedimentation of feed pellets is their terminal velocity. When a particle starts to fall in still water with zero initial velocity, it accelerates under the gravitational acceleration until the sum of the forces acting on the particle becomes zero and the particle reaches a constant falling velocity, called the terminal velocity. Although the column height of the fish tank is just below the average human size, another variable that controls the rate of a falling particle in a fluid medium such as fish activity and the inlet of water could also contribute to the rate of settling. When we look at this approach, we assume that there is zero activity in the tank and that particle will travel at constant velocity regardless of the parameter which contributes hugely on the trajectory of travel and settling before reaching the bottom. This is because we want to discover what flow rate would likely be keeping particles suspend for a longer period of time. Terminal velocity of feed pellet is one of the important parameters for the determination of their residence time in the column of the tank. Other main variables affecting terminal velocity are the size and shape of the particle (Clift R. G., 2005). As a result, in order to have a proper assessment of particle terminal velocity, it is necessary to quantify their size and shape. Feed pellets are known to have non-spherical and irregular shapes, with physical, chemical and mechanical characteristics significantly different from those of spherical particles (Khater & Ali, 2014). Nevertheless, feed particle have often been approximated as a sphere in numerical descriptions and observations strategies.

1.1 TERMINAL VELOCITY AND DRAG COEFFICIENT OF PARTICLE

1.1.1 Particle movement through fluid due to gravitational field

In settling and sedimentation, the particle is separated from the fluid by gravitational field forces acting on the particle. The density of particle, therefore, must differ than the density of medium.

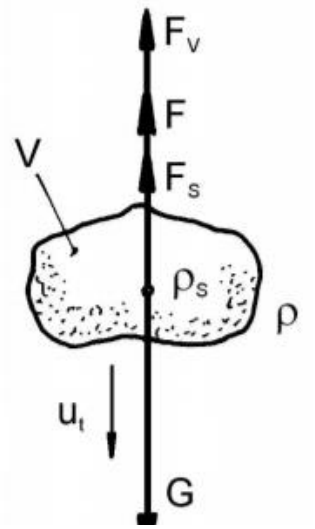

Figure 1. Force acting on particle as it settle down fluid medium

These differences in density will determine which direction sedimentation occurs. Settling of the sedimentary particles is controlled by many factors and can be classified by size and density. This chapter will describe what is known about settling velocity of the particle and how that has been translated into equations.

See fig 1. We will assume the motion of the particle is isolated at the stationary fluid medium. For the case of positive orientation in the direction of gravitational force, we can describe the motion according to Newton's second law for one-dimensional motion in scalar terms (all forces act in the vertical direction), in the form;

$$V\rho_s g - V\rho g \ - C_{Dt}\, S_P \rho \frac{u_t^2}{2} = V\rho_s \frac{du_t}{dt} \tag{1.1}$$

where V is the volume of particle, S_P is the cross-section of particle perpendicular to the direction of flow, ρ_s and ρ is the density of particle and fluid medium g gravitational acceleration, u_t is the instantaneous velocity of a particle with respect to the surrounding fluid and C_{Dt} is the drag coefficient of medium against motion of particle.

The term on the right-hand side of Eq. (1.1) expresses the time dependency of particle momentum. On the left-hand side, there are sequentially expressed forces acting on a particle: gravitational $G = mg$, buoyancy or Archimedes force $F_V = V\rho g$, and the resistance or drag force of the medium $F = C_{Dt}\, S_P \rho \frac{u_t^2}{2}$, which always acts against the velocity of particle.

1.1.2 Stationary particle movement – free settling velocity

In typical sedimentation columns, only a short time elapses (fractions of a second) from the start of the process to an equilibrium steady state of the forces acting on the particle, when the resultant of all the forces is equal to zero. Acceleration is therefore also zero and the particle moves uniformly onwards. If we assume that in Eq. (1.1), the density of the particle is greater than the density of fluid ($\rho_s > \rho$), the particle will move in the direction of gravitational acceleration at a constant velocity, which we will call sedimentation velocity u_t. From Eq. (1.1) we get

$$V(\rho_s - \rho)g = C_{Dt}\, S_P \rho \frac{u_t^2}{2} \tag{1.2a}$$

We further express the volume V_p and area S_P for the case of spherical particle by equation

$$\begin{aligned} V_p &= \frac{\pi d_s^3}{6} \\ S_P &= \frac{\pi d_s^2}{4} \end{aligned} \tag{1.2b}$$

where d_s is the diameter of particles determined by direct measurement or by sieve analysis (further chapter will explain more of these methods). After combining Eqs. (1.2a) and (1.2b) we obtain

$$C_D = \frac{4}{3}\frac{D(\rho_s - \rho)g}{u_t^2 \rho} \tag{1.3}$$

The drag coefficient is the most challenging parameter to determine since for a freely falling particle it depends on many parameters, including particle Reynolds number, shape, orientation and particle-to-fluid density ratio (Clift, Grace, & Weber, 2005). In sedimentation, just as in another hydrodynamic process, a Reynolds number is introduced Re by the relation for both spherical and non-spherical particle

$$\mathrm{Re} = \frac{u_t D \rho}{\mu} = \frac{u_t D}{\nu} \tag{1.4}$$

where μ designates the dynamic and ν the kinematic viscosity of medium. For the kinematic viscosity applies $\nu = \mu/\rho$.

(Stokes, 1851) showed that at $\mathrm{Re} \ll 1$, where inertial terms in the Navier-Stokes equations are negligible, Navier-Stokes equations can be simplified to a linear deferential equation, which can be solved analytically. At standard condition (i.e. moving with constant relative velocity in undistributed, unbounded and incompressible flow), for any solid spherical particle, the drag coefficient is

$$C_D = \frac{24}{Re} \tag{1.5}$$

At higher Reynolds number, the interactions between fluid and particles is highly non-linear and complex, and no analytical solution is available for estimating the drag coefficient, even for spherical particles for which shape quantification is not an issue. Thus, experimental measurements are the main source of information while numerical solution and boundary layer theory can provide additional information (Clift, Grace, & Weber, 2005).

1.1.3 Drag of non-spherical particles

The sedimentation of the non-spherical particle is generally more complex than for spherical particle although the dependency of the drag coefficient of non-spherical particles on the particle Reynolds number is very similar to that of sphere.

In general, at given particle Reynolds number, the average drag coefficient of falling non-spherical particle is higher than that of a sphere as a consequence of the influence by the shape, roughness,

orientation and particle to-fluid density ratio. As a result, the main challenge is to quantify the shape of particles through a *shape factor* that is well correlated with the drag coefficient.

Shape factors are dimensionless quantities used in image analysis and microscopy that numerically describe the shape of particle, independent of its size. The dimensionless quantities often represent the degree of deviation from an ideal shape, such as a circle, sphere or equilateral polyhedron (Wojnar L., 2000). Studies dealing with sedimentation and transport of particle commonly use shape factor of sphercity, introduced by Wadell (H. Wadell, 1934) introduce the concept.

$$\phi = \frac{s}{S} \tag{1.6}$$

Here s is the surface of a sphere having the same volume as a particle and S is the actual surface area of the particle. Shape factors value ranges from zero to one. A shape factor equal to one usually represents an ideal case or maximum symmetry, such as a circle, sphere, square or cube.

The most common models for estimation drag coefficient of non-spherical is introduce by (Haider & Levenspeil , 1989). The models of Haider and Levenspiel, Eq (1.6) is generalized correlation for drag coefficient of regular shape particles, which is based in Re and sphericity ϕ.

$$C_D = \frac{24}{\mathrm{Re}}(1 + b_1 Re^{b_2}) + \frac{b_3}{1 + \frac{b_3}{\mathrm{Re}}} \tag{1.7}$$

with the following definition of parameters b_i as

$$\begin{gathered} b_1 = \exp(2.3288 - 6.4581\phi + 2.4486\phi^2) \\ b_2 = 0.0964 + 0.5565\phi \\ b_3 = \exp(4.905 - 13.8944\phi + 18.4222\phi^2 - 10.2599\phi^3) \\ b_4 = \exp(1.4681 + 12.2584\phi - 20.7322\phi^2 + 15.8855\phi^3) \end{gathered} \tag{1.8}$$

1.2 EXPERIMENTAL METHODS FOR MEASUREMENT OF PARTICLE DRAG COEFFICIENT

Settling columns represent the most used technique for experimental determination of particle terminal velocity and drag coefficient (Isaacs & Thodos , 1967). In this technique, particles are released from the top of a vertical column, usually filled with a liquid (e.g. water-based mixtures), and its terminal velocity is measured (e.g. by stopwatch timing, video imaging) after it travelled for a *sufficiently* long distance, where particle acceleration becomes negligible. The required falling distance is dependent on several parameters including the particle size and shape and properties of the fluid (i.e. density and viscosity).

We implement the same methodology to determine the calculation of sedimentation velocity u_t from Eqs. (1.1-1.4) since it needs to be done experimentally. This is due to the fact that the sedimentation velocity u_t is contained in the definition of the resistance coefficient C_{Dt} as well as in Reynolds' number Re.

1.3 PARTICLE SIZE CHARACTERIZATION

As we mentioned earlier, characterizing particle of irregular shape can be complex procedure in order to obtain accuracy of measurement. Particle size of pellets is typically characterized based mechanical sieving, laser diffraction analysis and/or dynamic image analysis (DIA). Most common method and easy to implement is mechanical sieving down to 63 μm, while laser diffraction and DIA analysis can provide measurement at various size ranges between 0.1 μm and 30 mm.

Above-mentioned techniques are powerful tools for rapid assessment of bulk grain size distribution. However, they cannot be used to accurately derive important characteristic of individual particles, such as volume and surface area. These characteristics are what is most important for the determination of particle physical, mechanical and chemical behaviour, such as terminal velocity. For spherical particle, these parameter can be obtain directly by knowing the diameter, however, for irregular feed pellet particles, it is not that simple.

Other less common techniques used to characterized particle size include manual measurement. This method was recently used by (Khater & Ali, 2014). Author studies was carried to determine the physical and mechanical process of pellets. The dimension of pellets were measured using digital vernier caliper (Model TESA 1p65- Range 0-150 mm ± 0.01 mm, Swiss). The surface area and volume was simply calculated by measuring the height and radius of feed pellet. Although this methodology is an unorthodox to other available techniques, such as those that require sophisticated instrument where volume and surface area can be measured directly, we could implement the same method because it is less time consuming and some of those equipment are not available at all.

1.4 OBJECTIVE OF THIS WORK

Aquaculture studies cover a wide range of research based on the optimal effort to produce sustainability of fish production in order to increase the demands of protein's for human consumptions. Therefore, many different methodologies is implemented according to the type of findings that eventually would lead to increasing rate production, cutting cost by improving the design of the tank, changing control variable that effects fish welfare, etc.

For the first section, we have established a baseline where every aquaculture faces a common problem. Studies over the decade have a primary concerns on the effect of tank hydrodynamics. Tvinnereim, (1988) studied the influence of inlet design and impulse force on the current velocity and flow distribution in circular and octagonal tanks. Our primary objective is the trajectory of the fish pellet (particle) when injected inside the surface of the tank and observed. Reasons have been explained in the introduction sections. Attempt has been made to increase the suspension of bio-solids. Vertical baffles, installed perpendicular to the water flow could increase bottom velocities and reduce biosolid accumulation but interfere with fish handling and in some cases caused behavioral problems (Burley, 1985). In another approach, a pipe placed along the bottom of one side of the raceway jetted water along the tank bottom, thus establishing rotary circulation on the longitudinal axis of the tank. This provided self-cleaning properties (Watten and Beck, 1987; Watten and Johnson, 1990) but the costs of tank construction were high.

Computational Fluid Dynamics (CFD) has become a promising tool to create a platform for simulation-driven product development, without the need to produce working prototypes for testing. By solving the conservation equations for mass and momentum using CFD tools, comprehensive information on various flow features can be obtained and used to improve the flow conditions. The primary objective of this work is to study the trajectories of the particle (feed pellet) in a fish tank using the CFD-DPM approach and evaluating residence time distribution in the concerned fish tank. The internal fish tank geometry will also influence the flow pattern and thus particles motion. One of the most difficult part, as stated in previous section is to obtain the effective density of pellets. This is because the density of pellets also plays a major role in their trajectory during falling in the fluid flow domain.

The present work was carried out to fulfil the following objective summarized as follow:

a. Creating a lab-scale experiment to obtain basic properties of fish pellets to perform CFD analysis.

b. To utilize CFD-DPM approach in conducting steady analysis of particle trajectories injected from the surface of tank at different inlet velocity.

c. Comparing the obtained results with available literature and to propose further scope related to the present work.

CHAPTER II CFD-DPM

2.1 CFD SOFTWARE PACKAGES

CFD ANSYS Fluent package offer structured around the numerical algorithms that can tackle fluid flow problems. The packages code are constructed and separated into three elements, frequently:

1. Preprocessor
2. Solver
3. Post Processor

I would like to explain all the three elements briefly.

2.1.1 Preprocessor:

Preprocessor consists of geometry and mesh definition of a problem so that it could be easily interpreted by the solver section of the CFD.

Preprocessor consists of several stages such as

- Definition of the geometry of the region of interest i.e. **computational domain.**
- Grid generation the subdivision of the domain into several smaller, non-overlapping domains such as grids, cells (or control volumes).
- Selection the physical and chemical phenomenon that needs to be modelled.
- Definition of fluid properties.
- Specification of approximate boundary conditions.

2.1.2 Solver

There are three distinct streams of numerical solution techniques

- Finite element method
- Finite difference method
- Spectral methods.
- Finite volume method

We shall be primarily concerned with the finite volume method as the ANSYS FLUENT SOLVER depends on this method.

2.1.3 Post Processing

Post processing help us to interpret results using, for example, vector plots, line and shaded contour plots, 2D and 3D surface plots, particle tracking, trajectories, etc.

2.2 PRINCIPLES OF COMPUTATIONAL FLUID DYNAMICS

2.2.1 Introduction to governing equations

All CFD, in one form or another, is based on the fundamental governing equations of fluids dynamics – the continuity, momentum, and energy equations. The fundamental physical upon which all fluid dynamics is based:

1. Mass is conserved
2. Newton's second law, **F = ma**
3. Energy is conserved

This chapter is produced so that both author and reader could understand the meaning and significant of each of these equation to interpret the CFD results obtained by numerically solving these equations. These physical principles are applied to a model of the flow; in contrast, this application results in equations which are mathematical statement if particular physical principle, namely, the continuity, momentum, and energy equation. Each different model of the flow directly produces a different mathematical statement of the governing equations, some in conservation form and other in non-conservation form. Most of the differential equations in this chapter will mainly focus on the conservation form due to excess amount of information that would not be necessary for this work. This is because we are interested only on the forms of governing flow equations that are *directly* obtained from a flow model which is fixed in space. Finally, the physical boundary conditions and their appropriate mathematical statement will be developed. The governing equations must be solved subject to these boundary conditions.

2.2.2 The continuity equations

Applying the fundamental laws of mechanics to a fluid gives the governing equations for a fluid. The conservation of mass equation is

$$\frac{\partial \rho}{\partial t} + \nabla.(\rho \vec{u}) = 0 \qquad (2.1)$$

Where $\vec{u}$ is the flow velocity at a point on the control surface, $\vec{u} = f(x, y, z, t)$ and ρ is the density of fluid. Equation (2.1) is a *partial differential equation form of the continuity equation.* It was derived on the basis of an *infinitesimally small* element fixed in space. The fact that the element

was *fixed in space* leads to the specific differential form given in Eq. (2.1), which is called *conservation form*. For incompressible flows, Eq. (2.1) is simplified to

$$\nabla . \vec{u} = 0 \tag{2.2}$$

2.2.3 The momentum equation

In this section, we apply another fundamental physical principle to a model of flow, namely:

Physical principle: **F = ma** (Newton's second law) (2.3)

The resulting equation is called the *momentum equation.* Newton's 2nd law, expressed above, when applied to the moving fluid element says that the net force on the fixed fluid element equals its mass times the acceleration of the element. This is a vector relation, and can be split into three scalar relations along the $x, y,$ and z-axes. We will not get into detail for the derivation of these equation and therefore, the simple form is summarized as follow

$$F_x = \left(-\frac{\partial p}{\partial x} + \frac{\partial \tau_{xx}}{\partial x} + \frac{\partial \tau_{yx}}{\partial y} + \frac{\partial \tau_{zx}}{\partial z} \right) dx\, dy\, dz + \rho f_x\, dx\, dy\, dz \tag{2.4}$$

Note that the equation above is only represent the left-hand side of Eq. (2.3). Considering the right-hand side of Eq. (2.1), recall that the mass of the fluid element is fixed and is equal to

$$m = \rho\, dx\, dy\, dz \tag{2.5}$$

Also, recall that the acceleration of the fluid element is the time-rate-of-change of its velocity. Hence, the component of acceleration in the x-direction, denoted by a_x, is simply the time-rate-of-change of u; since we are following a moving fluid element, this time-rate-of-change is given by the substantial derivative. Thus

$$a_x = \frac{Du}{Dt} \tag{2.6}$$

Combining Eqs. (2.4-6), we obtain

x-component of the momentum equations:

$$\rho \frac{Du}{Dt} = -\frac{\partial p}{\partial x} + \frac{\partial \tau_{xx}}{\partial x} + \frac{\partial \tau_{yx}}{\partial y} + \frac{\partial \tau_{zx}}{\partial z} + \rho f_x \tag{2.7a}$$

y-component of the momentum equation:

$$\rho \frac{Dv}{Dt} = -\frac{\partial p}{\partial x} + \frac{\partial \tau_{xy}}{\partial x} + \frac{\partial \tau_{yy}}{\partial y} + \frac{\partial \tau_{zx}}{\partial z} + \rho f_y \tag{2.7b}$$

z-component of the momentum equation:

$$\rho \frac{Dw}{Dt} = -\frac{\partial p}{\partial x} + \frac{\partial \tau_{xz}}{\partial x} + \frac{\partial \tau_{yz}}{\partial y} + \frac{\partial \tau_{zz}}{\partial z} + \rho f_z \tag{2.7c}$$

Equations (2.7a-c) are the Navier-stokes equations in *non-conservation* form. In the late seventieth century Isaac Newton stated that shear stress in a fluid is proportional to the time-rate-strain, i.e. velocity gradient. Such fluid are called *Newtonian* fluids. The Navier-Stokes equations in symbolic tensoril form follows:

$$\rho \left[\frac{\partial \vec{u}}{\partial t} + (\vec{u}.\nabla)\vec{u}\right] = -\nabla p + \rho \vec{f} + \nabla.\vec{\vec{\tau}} \tag{2.8}$$

Where $-\nabla p$ is the pressure force, $\vec{f}$ is the body force per unit mass and $\nabla.\vec{\vec{\tau}}$ is the viscous tensor. The viscous stress tensor $\nabla.\vec{\vec{\tau}}$ for the case of Newtonian fluid can be written as

$$\tau_{ij} = \mu\left(\frac{\partial u_i}{\partial u_j} + \frac{\partial u_j}{\partial u_i} - \frac{2}{3}(\nabla.\vec{u})\delta_{ij}\right) \tag{2.9}$$

where δ_{ij} is the *Kronecker-Delta* operator which is equal to 1 if $i = j$, otherwise equals to zero, x_i denoted mutually perpendicular coordinate directions and μ is the molecular viscosity coefficient.

2.2.4 The energy equation

We now reach to the final section where the fundamental physical principle state as follow

Physical principle: Energy is conserved

Energy equation is a mathematical statement representing the conservation of energy principle and for incompressible flows can be written as:

$$\rho c_P \left[\frac{\partial T}{\partial t} + \vec{u}\nabla\, T\right] = \lambda \nabla^2 T + \dot{q}^{(g)} + \vec{\vec{\tau}}:\vec{\vec{\Delta}} \tag{2.10}$$

where c_P is specific heat at constant pressure, T is absolute temperature, $\vec{\vec{\tau}}$ is dynamic stress tensor, $\vec{\vec{\Delta}}$ is symmetric part of the velocity gradient tensor and $\dot{q}^{(g)}$ represents internal heat sources or sinks. Eq. (2.5.1) is called Fourier-Kirchoff equation.

2.2.5 Comment on the governing equations

These equations along with the conservation of energy equation form a set of coupled, nonlinear partial differential equations. It is not possible to solve these equations analytically for most engineering problems and hence they are very difficult to solve. To date, there is no general closed-form solution to these equations. However, we could solve these equations numerically by solving

a problem for a particular case at discrete points. The utilized discrete points will enable the transformation of partial differential equation to solvable algebraic equations. There are numerous methods available to do this discretization.

A common discretization scheme utilized in CFD analysis is the *Finite Volume Method*, which is based on dividing the computational domain into control volumes. The differential equations are integrated over the control volumes and divergence theorem is applied. To evaluate the derivatives, the values at the control volume faces are required, which is based on some assumption about its variation. The result is a set of algebraic equations one for each control volume which is solved iteratively. In the present work, ANSYS Fluent software package was used for CFD analysis which is based on Finite Volume Method.

2.2.6 Turbulent modelling

In turbulent flow, the field properties become random and chaotic fluctuation of transported quantities, mainly velocity, temperature and pressure. Compared to laminar flow, the flow of turbulence is linked directly to high Reynolds number, where inertial forces dominated viscous forces. This ultimately become a challenge when solving turbulent flow for Navier-Stokes equation. It is standard practice, a detailed description of the turbulent eddies is not needed, and a knowledge of what happens to the flow field in an average sense is sufficient. Any property can be written as the sum of average and fluctuation by using Reynolds decomposition.

$$u = \bar{u} + u' \tag{2.11}$$

where $\bar{u}$ is the time-average of velocity. This method of analyzing a turbulent flow, known as the Reynolds averaging approach, is the most commonly adopted for engineering CFD studies. In the Navier-Stokes equation, the velocity fluctuation with respect to time is separated from the mean flow velocity and pressure of fluid by averaging of the Navier-Stokes equation. The resulting equation is called Reynolds-Averaged Navier-Stokes (RANS). RANS equation can be written (in tensor notation) (White, 1974),

$$\frac{\partial}{\partial t}\left(\rho\bar{u}_j\right) + \frac{\partial}{\partial x_j}\left(\rho\bar{u}_i\bar{u}_j\right) = -\frac{\partial\bar{p}}{\partial x_j} + \frac{\partial}{\partial x_j}\left(\mu\frac{\partial\bar{u}_i}{\partial x_j}\right) + \frac{\partial \mathrm{R}_{ij}}{\partial x_j} \tag{2.12}$$

where R_{ij} is the Reynolds stress tensor which describe the component of the total stress tensor in a fluid obtained from the averaging operation over Navier-Stokes equation to account for turbulent fluctuations in fluid momentum. Equation (2.11) is not fully develop yet due to new unknown

introduced such as Reynolds stress tensor and turbulent fluxes. Additional equation is required so we can close the system by developing turbulent model (see chapter 4).

2.3 PRINCIPLE OF DISCRETE PHASE MODEL

2.3.1 Eulerian verses Lagrangian model

In multiphase particle CFD modeling, there are two commonly used approaches: the Eulerian model and the Lagrangian model. The models differ their treatment if the second particle phase. The Eulerian model treats the particle phase as a second continuum phase calculated from mass conservation principles (Lai & Chen, 2007). In this case, the solution is typically interpreted in terms of a concentration field, since individual particles cannot be tracked in this method. The Lagrangian model differs from the Eulerian model in that it treats the second phase as a discrete collection of individual particles. The trajectory of each particle is calculated based on Newton's Second Law where the momentum imparted comes from the interaction with the continuous phase as well as particle body forces. The primary forces considered are drag forces, pressure gradients forces, Basser forces, virtual (added mass) force, gravitational forces, and buoyancy force (Crowe, Schwarzkopf, Sommerfeld , & Tsuji, 2011). While this is not a complete list of forces, cumulatively, they comprise a high majority of forces which can affect particle trajectories. The resultant force is then calculated at discrete time intervals and the particle is advanced according to the force. This is why the Lagrangian model is sometimes referred to as the "discrete phase model" (DPM).

Each model has specific advantages and disadvantages depending on the requirements of the simulation. For cases in which a concentration field is the main priority, the Eulerian model is preferred since its method of calculation innately generates a concentration profile. In contrast, a case study in which concentration is not the primary concern, but rather particle history is desired, the Lagrangian model is preferred. In terms of efficiency, the Eulerian model requires significantly less computational power since it solves for a single continuum, while the Lagrangian model must solve for multiple independent particle trajectories. In many simulations of particle dispersion with larger heavy particles ($\rho_{particle} >> \rho_{fluid}$), Lagrangian models are used because the particle behaviour is significantly different from that of the continuum phase due to the effects of gravity and buoyancy (Wang & Stock, 1993). Since this research focuses on both heavy particles and tracking where the particle history is of high importance, the Lagrangian method will be used.

2.3.2 Modeling Discrete Phase

Computation of simulation of the discrete second phase in the Lagrangian frame of reference is included in ANSYS Fluent package. The second phase consists of spherical particles (which may be taken to represent droplets or bubbles) dispersed in the continuous phase. ANSYS Fluent computes the trajectories of these discrete phase entities. The modeling of discrete the phase is the trajectories of particle-based on Lagrangian formulation which include the discrete phase inertia, hydrodynamic drag, and the force of gravity, for both steady and unsteady flows. The prediction of the effect of turbulence on the dispersion of particles due to turbulent eddies also might be also taken into account.

These modeling capabilities allow ANSYS Fluent to simulate a wide range of discrete phase problems. The physical equations used for these discrete phase calculation are described in the following section.

2.3.3 Simplified assumptions of Discrete Phase Model

The discrete phase formulation used by ANSYS Fluent contains the assumptions that the second phase is sufficiently dilute that particle-particle interaction and the effect of the particle volume fraction on the gas phase are negligible. In practice, these imply that the discrete phase must be present at a fairly low volume fraction, usually 10-12%. In general, this limit is far too high and does not fulfill the requirement of the ratio between the momentum response time and collisional time. The DPM model is however often used for dense dispersed flows as well. Care should be taken when interpreting the results. Interparticle interactions might be important and Dense DPM model variatns should be used in such cases.

The steady-state DPM model cannot be applied for continuous suspension of particles but well suited for flows in which particle streams are injected into a continuous phase flow with well-defined entrance and exit conditions. For cases, in which the particles are suspended indefinitely in the continuum (e.g. stirred tanks), the unsteady DPM modeling should be used instead.

2.3.4 Particle Force balance

The trajectory is calculated by integrating the particle force balance equations, which is written in a Lagrangian reference frame. This force balance equates the particle inertia with the forces acting on the particle and can be written (for the x direction in Cartesian coordinates) as (ANSYS, Inc, 2012)

$$\frac{du_p}{dt} = F_D(u_i - u_P) + \frac{g_x(\rho_P - \rho)}{\rho_P} + F_x \tag{2.13}$$

where F_x is an additional acceleration (force/unit particle mass), $F_D(u_i - u_P)$ is the drag force per unit particle mass and

$$F_D = \frac{18\mu}{\rho_P d_p^2} \frac{C_D \mathrm{Re}}{24} \tag{2.14}$$

Here, u is the fluid phase velocity, u_p is the particle velocity, μ molecular viscosity of the fluid, ρ is the fluid density, ρ_P is the density of particle and d_p^2 is the particle diameter. Re is the relative Reynolds number, which is defined as

$$\mathrm{Re} \equiv \frac{\rho d_p |u_P - u|}{\mu} \tag{2.15}$$

For smooth spherical particles, ANSYS Fluent uses equation by (Morsi, 1972).

$$C_D = a_1 + \frac{a_2}{\mathrm{Re}} + \frac{a_3}{\mathrm{Re}^2} \tag{2.16}$$

where constant a_1, a_2, and a_3 are determined for different range of Re. The drag coefficient, C_D, change with relation to particle and flow characteristics. Since we are dealing with irregular shape particles, the equations by (Haider & Levenspeil , Drag Coefficient and Terminal Velocity of Spherical and, 1989) are used as stated in chapter 1.

Other forces might be irrelevant to the objective of this work. More information on the equation of motion of particles can be found in the article (ANSYS, Inc, 2012).

2.3.5 Definition of coupling between phases

When determining particle characteristics, the level of interaction between the particle phase and the fluid phase must be determined. This interaction is typically broken into a series of "coupling" scenarios: 1-way coupling, 2-way coupling, and 4-way coupling. The one-way coupling means that the particle movement is affected by the flow; particle movement does not affect the surroundings fluid whereas in the two-way coupling, not only the particle movement is affected by the flow, but the flow around the particle is also affected by the presence of a particle. The major feedback is noted in turbulence damping due to buoyancy effects (Elghobashi, 1994). Regardless of whether one-way or two-way coupling methods are used, the solutions are based on a partitioned method where separate solutions for the different physical fields are prepared. One field that has to be solved is fluid dynamics, the other is structure dynamics. Four-way coupling takes into account also particle-particle and particle-wall interaction. This is beyond the scope of this work.

CHAPTER III EXPERIMENT AND RESULT

3.1 SAMPLE

Two different particles (pellet) types are selected for this study (Table 1). The particle or pellet is classified based on the physical and mechanical properties. There are no standards to distinguish between pellets except for the based organic compound properties such as protein ratio and pellet size.

Table 1. Sample of test pellets provided by University of South Bohemia, FFPW.

Batch	Code	d_{eq}	Protein ratio		
			Fish-based, %	Lipids, %	Insects, %
1	TM0	0.0035	100	100	0
2	TM75	0.0034	25	25	75

20 random pellets were selected from each batch. Each pellet is measured using a ruler that is attached directly to each image taken by a camera and later on measure individually from one another. Each picture correspond to the number assigned on each pellet. Assuming the pellet characteristic having the equivalent diameter of the sphere, we only took consideration of the width of pellet as our characteristics dimension of diameter (see figure 2).

3.2 VERTICAL COLUMN SET UP

Figure 3 shows a schematic representation of the experimental setup. In each experiment, an individual particle was dropped inside the graduation cylinder while being filmed with a digital phone camera. The camera is placed about 35 cm away from the setup test. A white background is placed behind the test scheme in order to detect and avoid any background noises. Although the setup is relatively simple, it is enough to understand the particle behavior on free failing since were dealing with small scale setup.

In order to produce a uniform velocity of a particle falling inside the column, we will start the timing when particle crosses the blue line and end the time when particle cross over the red line. Thus, approximately, the particle will travel at a distance of 22.4 cm as indicated in Fig 3.

Terminal velocity, or in other words zero acceleration must be achieved as is one of the conditions because measured drag coefficient of accelerating or decelerating particles are different than those measured in standard conditions (Clift, Grace, & Weber, 2005).

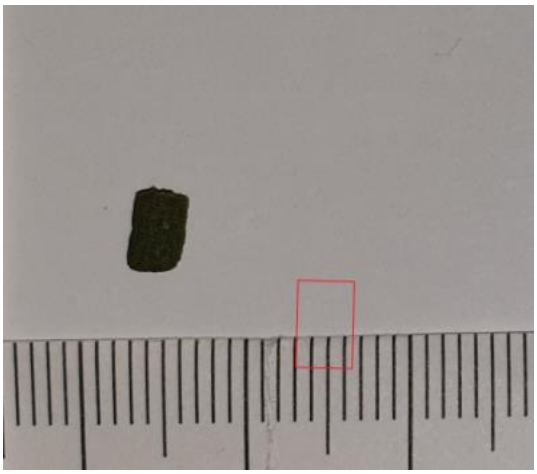

Figure 2. Sample pellet TM0 – The red box is an outline parameter of the sample measured against real scale

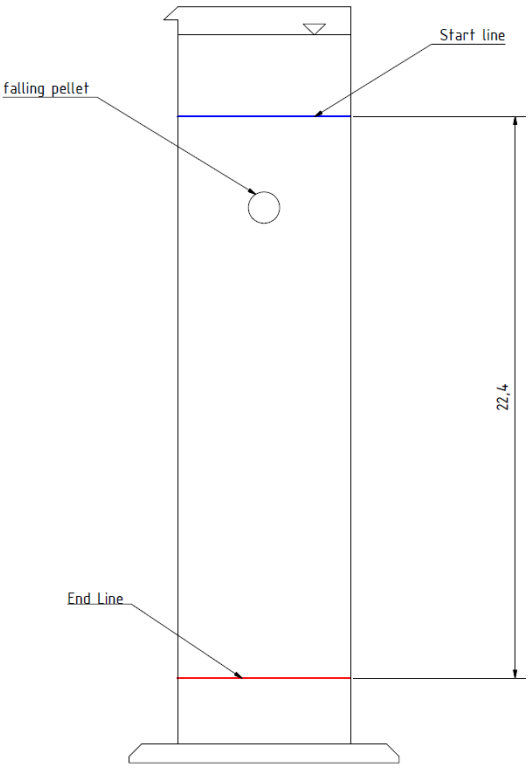

Figure 3. Setup sketch to illustrate feed pellet settling in water column (tap water was used). This experiment was used to determine settling velocity and effective density of the feed particle.

3.3 RESULT

3.3.1 Obtaining density based on settling velocity.

Table (2) and (3) summarized the measured settling velocities of 10 selected pellets from each batch. The fluid (water) used in our calculations corresponded to temperature 20°C (density 998.2 kg/m^3 and kinematic viscosity 11.004 × 10^{-6} m^2/s). Because the pellet is porous organic material, one may argue that during settling the pellet absorb water which dramatically changes the density and therefore, it is important to find out their effective density in the water. Assuming that the characteristic size (diameter) of particle is known, we could express the effective density of the particle from Equation (1.3) as

$$\rho_P = \rho_f + \frac{4}{3}\frac{D(\rho_s - \rho)g}{u_t^2 \rho} \tag{3.1}$$

Since the settling column is rather short to any other comparative settling test analysis such as one in a recent study (Karabulut & Yandi, 2011) where one-meter column is used, the pellet still not capable of producing any differences unless the column height is increased, lower viscosity or different material properties of the pellet. Nevertheless, we conducted a second test where the pellet was now soaked in water for about 15 minutes before and then dry to soak for a minute to take a second measurement after soaking before settling into the column the same as the first test whilst maintaining the condition relatively the same. The result is present in the Table (2) and (3).

Table 2. Experimental result of TM0 from batch 1

Particle Number	Particle Approx Dia. (mm)	Time (s)	Velocity (cm/s)	Re [-]	C_d [-]	density (kg/m^3)
11	3.5	3.667	6.109	212.947	0.8845	1070.2
12	3.9	3.466	6.463	251.044	0.8515	1067.8
13	3.5	3.57	6.275	218.733	0.8786	1073.6
14	3.2	7.1	3.155	100.556	1.1519	1025.5
15	3.5	4.967	4.510	157.213	0.9679	1041.1
16	3.8	4.566	4.906	185.679	0.9184	1042.6
17	3.5	3.933	5.695	198.545	0.9011	1061.9
18	3.4	4.56	4.912	166.352	0.9500	1049.7
19	3.5	4.8	4.667	162.683	0.9569	1043.6
20	3.2	4	5.600	178.486	0.9293	1067.7
Average	**3.5**	**4.4629**	**5.229**	**183.224**	**0.9390**	**1054.4**

Table 3. Experiment result of TM75 from batch 1

Particle Number	Particle Approx Dia. (mm)	Time (s)	Velocity (cm/s)	Re [-]	C_d [-]	density (kg/m3)
1	3.9	5.2	4.308	167.331	0.9482	1032.6
2	2.9	3.7	6.054	174.868	0.9351	1088.4
3	3.5	3.9	5.744	200.225	0.8990	1062.9
4	3.5	3.9	5.744	200.225	0.8990	1062.9
5	3	3.367	6.653	198.789	0.9008	1099.6
6	3.5	2.966	7.552	263.276	0.8434	1103.1
7	3	5.067	4.421	132.094	1.0302	1049.4
8	3.8	2.6	8.615	326.080	0.8148	1119.7
9	3.9	3.667	6.109	237.284	0.8619	1061.1
10	3	5.1	4.392	131.240	1.0328	1048.9
Average	**3.4**	**3.9467**	**5.959**	**203.141**	**0.9165**	**1072.9**

Karabulut and Yandi, (2011) introduce a methodology that is slightly different compared to another conventional method such as image analysis and pycnometer. To measure the density of pellet with

an accuracy of 0.1%, Karabulut (2011) construct a device based on Mercury Displacement Method (MDM). The average density of 6 mm pellet is 1.0936 g cm^{-3} and the peak value is about 1.09 g cm^{-3}. The result obtain was roughly produced by density distribution diagram. The authors also stated that any measurement which has a percentage error greater than 2% will produce greater density difference ($\rho_p - \rho$). For the purpose of the present work, we were going to assume that all conditions criteria are met and therefore, instead of directly determining the density based on pellets size and mass, and the limited equipment available, we can obtain the density of the experiment numerically based on Reynolds number Re and drag coefficient present by (Haider & Levenspeil , Drag Coefficient and Terminal Velocity of Spherical and, 1989) C_D from Eqs. (1.4) and (1.7) respectively as summarized in table (2)-(5).

Table 4. TM0 after soaking for 15 minutes and new settling velocity

Particle Numer	Particle Approx Dia. (mm)	Time (s)	Velocity (cm/s)	Re [-]	C_d [-]	density (kg/m^3)
1	4	4.9	4.571	182.129	0.9236	1035.0
2	4.3	9.6	2.333	99.934	1.1550	1009.4
3	4.8	8.733	2.565	122.629	1.0604	1009.3
4	4.2	10.467	2.140	89.524	1.2136	1008.3
5	4.5	9.197	2.436	109.164	1.1120	1009.4
6	4.9	13.867	1.615	78.837	1.2885	1003.4
7	4.3	5.034	4.450	190.577	0.9115	1030.2
8	4.4	7.4	3.027	132.659	1.0286	1014.5
9	4.5	7.967	2.812	126.018	1.0491	1012.3
10	4.6	6.2	3.613	165.531	0.9515	1018.8
Average	**4.45**	**8.3365**	**2.956**	**129.700**	**1.0694**	**1015.1**

Table 5. TM75 after soaking for 15 minutes and new settling velocity

Particle Numer	Particle Approx Dia. (mm)	Time (s)	Velocity (cm/s)	Re [-]	C_d [-]	density (kg/m^3)
11	4.5	4	5.600	250.996	0.8515	1043.5
12	4.5	5.633	3.977	178.233	0.9297	1023.1
13	4	5.4	4.148	165.265	0.9520	1029.5
14	4	4.367	5.129	204.358	0.8941	1043.1
15	4	5.866	3.819	152.136	0.9788	1025.4
16	3	4.34	5.161	154.222	0.9742	1064.2
17	3.2	4.906	4.566	145.525	0.9942	1047.6
18	4.1	4.733	4.733	193.269	0.9079	1036.1
19	4.1	4.403	5.087	207.754	0.8902	1041.1
20	3.9	4.3	5.209	202.353	0.8964	1045.8
Average	**3.93**	**4.7948**	**4.743**	**185.411**	**0.9269**	**1039.9**

3.4 DISCUSSION

We mention in the previous chapter that in order to characterize particle (fish pellet) based on numerous methodology available, we will choose the most efficient and less time-consuming. Again, characterizing of irregular particle especially the one is lack of standardized is harder to define. The method use from sieve analysis was not accurate. One of the main reasons is that the pellet that shows the highest distribution has a missing sieve in which the experiment cannot continue and must come with an alternative method. We also cannot implement the image analysis method because the equipment was not available at the time and therefore we were stuck to the simplest methodology which is the classic ruller and relying heavily on the visual capability which to estimate has a percentage error rate of 2-5% error. Nevertheless, the experiment proceeds and the result obtained was not far from other published studies in similar cases.

CHAPTER IV CFD-DPM MODELLING

4.1 NUMERICAL METHOD AND MODEL DESCRIPTIONS

4.1.1 Introduction

In CFD analysis, the necessary condition prior to simulation is a modeled geometry defining the fluid domain with appropriate boundaries. The geometrical parameters of the model are selected with recent published studied as shown in Fig 4 (Lika et al., 2015). They aim to determine the ideal condition of *European Sea Bass* having a significant effect on different tank geometry (2000, 500, 40 L) on growth, survival, and stress. A dynamic energy budget (DEB) model was used to analyze the result. The author's findings show that they are no indication of correlations between the survival of fish tank-rearing volume although the effect does differ when it comes to the growth of fish on their feeding regime. Smallest tank volume shows to have lower growth compare to the big one which means that we would select 500l tank for the purpose of our research as shown in Fig. 4. Water is the main fluid for the research and we would use the same variable to keep things in perspective.

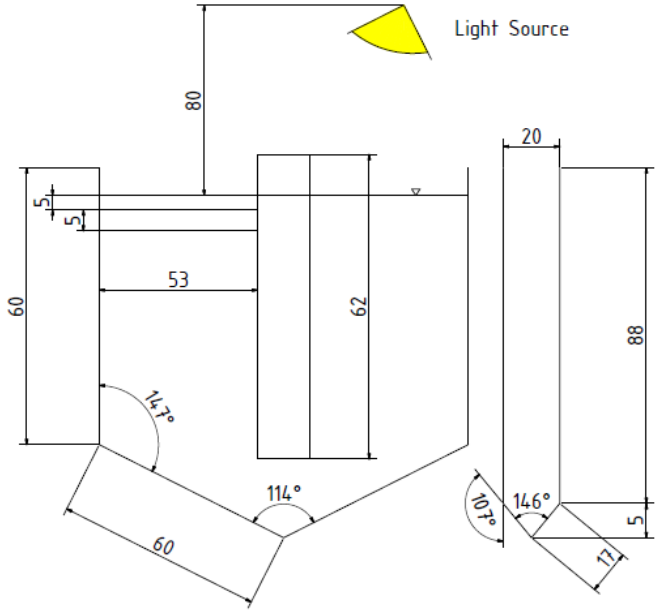

Figure 4. 500l Tank Geometry – unit in cm *(Lika & M. M. Pavlidis, 2015)*

Ipek (2019) investigated different modeled geometry tank that is listed by Lika et al., (2015) with the aid of Computational Fluid Dynamics (CFD) using Spalart-Allmaras, k-ω, and k- ε turbulent model to obtain the ideal flow rate that is suited for the condition of growth performance by the fish. The authors reported that the k- ε turbulent model is the best to match for good distribution of velocity in of the 500l tank that is used for the experimental procedure.

For the preceding of this chapter, we will portray the same approach present in Ipek (2019) work. One of the reason is to avoid the same explanation that is already been state in the paper presented, although the basic has to be mention to capture the best condition for the setup of simulation and also to direct to the objective of this work which focuses mainly on the particle behavior acting on different flow rate as we mention in chapter I.

4.1.2 Tank Geometry

The geometry obtained in ANSYS Design Modeler is shown in Figure (5) with inlet at the bottom and outlet through a pipe close to the surface. There is a draft tube in the center of the tank with rectangular holes which are covered by a net to prevent small fish being washed out (the impact of the net on flow pattern was neglected in our simulations).

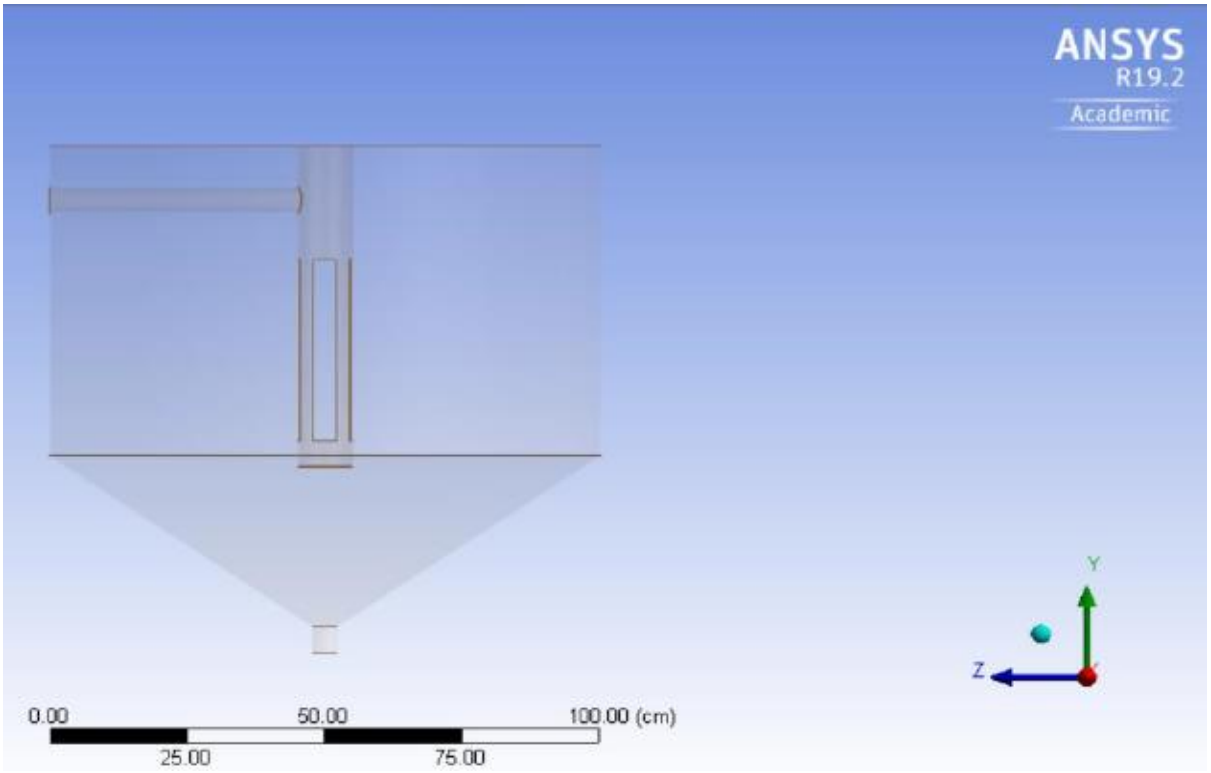

Figure 5. Geometrical Model of Fish Tank by Design Modeler ANSYS Fluent

4.1.3 Computational mesh and the quality

The first step in the CFD solution is the generation of a mesh that defines the cells on which flow variable (velocity, pressure, etc.) are calculated throughout the computational domain. The mesh used in this chapter is generated with the ANSYS package.

In general, CFD codes can run either structured or unstructured mesh. Most people will dislike unstructured meshes due to lack of direct control over the mesh and to the fact that much more data points and cells are produced than their structured counterparts. On the other hand, unstructured meshes are mostly automated, much easier to produce, and in more than numerous occasions are

the only ones possible (especially for large scale highly complex geometry for industrial applications). However, there are some advantages to structured meshing. In boundary layers, where flow variables change rapidly normal to the wall and highly resolved mesh are required close to the wall, structured mesh enables much finer resolution than do unstructured grids for the same number of cells.

We must emphasize that regardless of the type of mesh you choose (structured or unstructured) it is the quality of the mesh, many aspects of the mesh have a vital contribution to simulation accuracy, and include among others the type of physics models simulated, the details of the solution to the particular simulation, chosen discretization scheme and geometric mesh properties having to do with cell growth, smoothness, proximity and curvature attributes, stretching, featured angles, etc. This section has no intention of presenting an exhaustive list of metrics, but to name a few (orthogonality, skewness, aspect-ratio) as conceptual means in the evaluation of mesh quality and its impact on obtaining an accurate solution.

In particular case, you must always be careful that individual cells are not highly skewed, as this can lead to convergence difficulties and inaccuracies in the numerical solution. Other factors affect the quality of the mesh as well. For example, abrupt changes in cell size can lead to numerical or convergence difficulties in the CFD code. Also, cells with a very large aspect ratio can sometimes cause problems. While you can often minimize the cell count by using a structured mesh instead of an unstructured mesh, a structured mesh is not always the best choice, depending on the shape of the computational domain. You must always be cognizant of mesh quality. Keep in mind that a high-quality unstructured mesh is better than a poor-quality structured mesh.

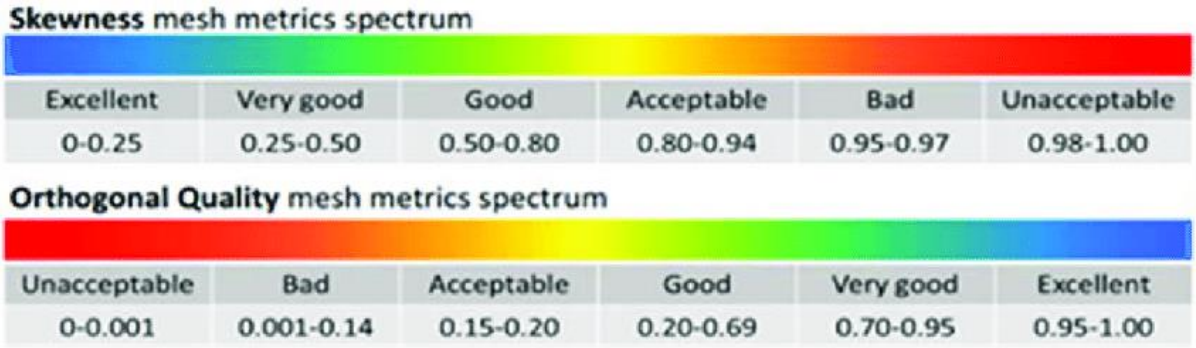

Figure 6. Skewness and orthogonal quality mesh metrics spectrums.

Table (6) shows the values of three different size of mesh element which is taken from Ipek (2019). The author generated these meshes by global element size option provided in ANSYS Fluent Package.

Table 6. Example of mesh quality measures for the generated grid (mesh) according to Ipek (2019).

Global Element size	Number of Elements	Nodes	Min. Orthogonal Quality	Max. Skewness Quality	Max Aspect Ratio
50 mm	156800	3016	0.6799	0.93201	16.041
30 mm	284907	52954	0.6385	0.936614	18.428
23 mm	487373	88343	0.6028	0.937796	23.82

It was mention that the author generates tetrahedral mesh before decreasing further the element size by transforming into a polyhedral mesh using ANSYS Fluent solver to improve the quality of the mesh and obtain better convergence result. One of the purposes is to reduce iteration time and faster simulation.

In the case of presented work, we created only one mesh in ANSYS meshing element with 907 600 of tetrahedral elements before the conversion with aid of Fluent solver to the polyhedral mesh which produces to reduce mesh element for refinement which is 258 000 mesh element in this conversion. The obtained values of the mesh quality measures for the generated mesh of modeled geometry as shown in Fig. 5. The discretized mesh element can be seen in Figure (7).

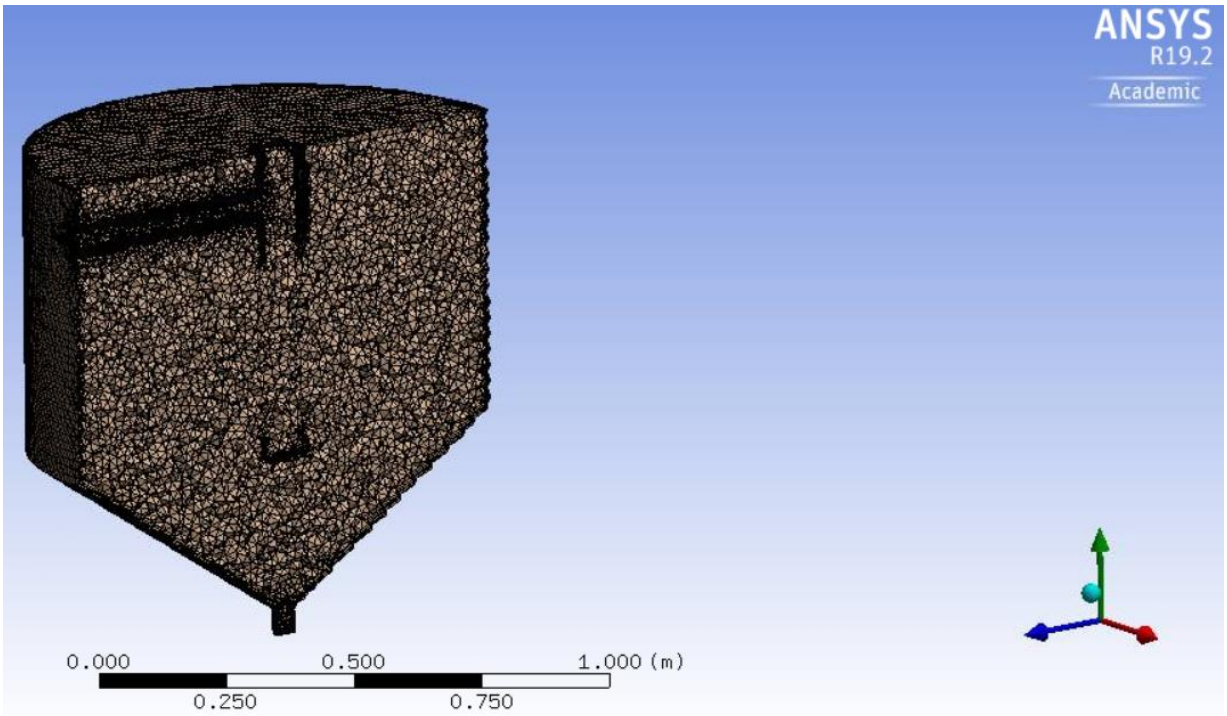

Figure 7. Meshing of Modelled Geometry.

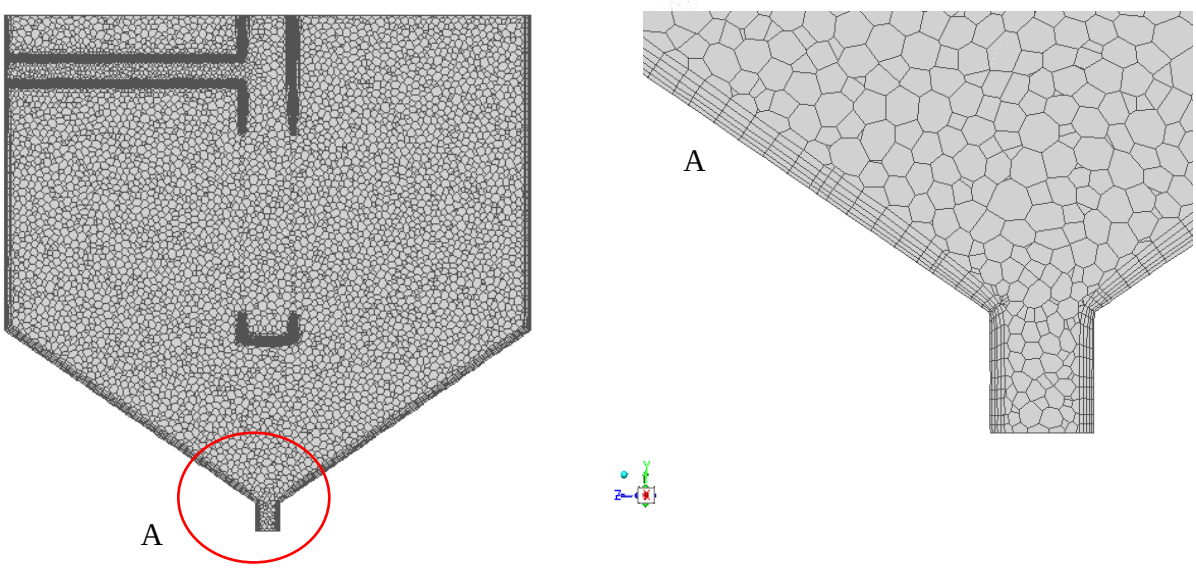

Figure 8. Illustration of polyhedral mesh of the fish tank used in CFD simulation. Total number of mesh elements after the polyhedral conversion was 258 000

Table 7. Quality of two different mesh depending on their type of meshing

Qaulity Measure	Tetrahedral mesh	Polyhedral mesh
Element	907 600	258 000
Maximum Skewness	0.9970	N/A
Minumum Orthogonal Quality	0.100	0.126
Maximum Aspect Ratio		7.988e+01

4.1.4 Grid Convergence Index

The evaluation of spatial (grid) convergence is a method to determine ordered discretization error in a CFD simulation. We implied the word “grid” here because it is more commonly referred to in CFD community. The method involves performing the simulation on two or more successively finer grids. The refinement of the grid results in an increase in the number of mesh elements and a decrease in the cell size present in the flow domain. The refinement can be spatial and/or temporal. The temporal refinement deals with the reduction in the size of the time step. As the grid is refined, the spatial and temporal discretization errors should asymptotically approach zero, excluding the round-off errors.

Methods for examining the spatial and temporal convergence of CFD simulations are presented in the book by (Roache, 1998). They are based on the use of Richardson’s Extrapolation suitable for analyzing the grid convergence. This method works by determining the Grid Convergence Index (GCI) and use these values for further evaluation of the different levels of grids required. Whether

or not this theory hold to improve the accuracy of measurement, the objective is to measure the uncertainty of the grid convergence.

The GCI can be computed using two levels of the grid; however, three levels are recommended to accurately estimate the order of convergence and to check that the solutions are within the asymptotic range of convergence. The GCI value for a particular grid-level indicates the inaccuracy in the obtained solution from that of an exact solution.

The Readers new to the concept of discretization error estimation are encouraged to review the summary provided on the web (NASA, n.d.). In the presented work by (Ipek, 2019), the GCI was evaluated to determine the appropriate mesh size for conducting unsteady and transient flow analysis with reasonable accuracy.

Since we are producing only one level of mesh or grid in this case, GCI evaluation is not going to work because as mention earlier that GCI can be computed at least by producing two or more refinements of grids. If reader is interested in the derivation of the equation explain in this section, (KWAŚNIEWSKI, 2013) provide the basic concept of grid convergence index. However, the method still needs to be mention. As mention earlier, there is no viable methodology to obtain "good quality" of meshing but we can estimate the discretization error and observed the rate of convergence so that engineers whose lacking in experience and those with experience seeking for confirmation of validation and verification of their simulation have a better judgment over the conventional trial-and-error.

4.1.5 Turbulent modelling based on RANS

The dimensions, geometry and the configuration of the inlet flow of circular fish tank shown in figure (6) ensure the flow domain inherently turbulent, which requires turbulence modelling. RANS is based on the Reynolds decomposition according to which a flow variable is decomposed into mean and fluctuating quantities. When the decomposition is applied to the Navier-Stokes equation an extra term known as the Reynolds Stress Tensor arises and a modeling methodology is needed to close the equations as explained in the previous chapter. The "closure problem is apparent as higher and higher moments of the set of equations may be taken, more unknown terms arise and the number of equations never suffices.

Two approaches can be used in order to obtain a closed form of equations that contain only the mean velocity and pressure, and this model can be divided by two categories that are Reynolds Stress Models (RMS) and Eddy Viscosity Model. The Reynolds stress is directly solve via transport equation given in Eq. (4.1) modeled by turbulence models which employ Boussinesq hypothesis by introducing the concept of eddy turbulent viscosity.

The Boussinesq assumption state that the Reynolds stress tensor, τ_{ij}, is proportional to the trace-less mean strain rate tensor S_{ij}^{*}, and can be written explicitly as

$$\rho\overline{u}_i^{\prime}\overline{u}_{j^{\prime}} = \mu_t\left(\frac{\partial U_i}{\partial x_j}+\frac{\partial U_j}{\partial x_i}-\frac{2}{3}\frac{\partial U_k}{\partial x_k}\delta_{ij}\right)-\frac{2}{3}\rho k\delta_{ij} \tag{4.1}$$

The role of turbulent modeling is essential to describe the turbulent (eddy) viscosity. There are several turbulence models utilized in the CFD analysis such as the Spalart-Allmaras model, the $k-\epsilon$ models, and the $k-\omega$ models. The Spalart-Allmaras model is not sufficient to do this due to its inability to compute the flow shear and anisotropic turbulence. Out of the widely used two-equation models, the Realisable k _ ε model exhibits superior performance in capturing the streamline curvature, rotation, recirculation and round jets, which makes it suitable for the present study.

4.1.6 Realizable $k-\varepsilon$ model

The term realizable means that the model satisfies certain mathematical constraints on the Reynolds stresses, consistent with the physics of turbulent flows. The benefits of choosing this model are due to the provision superior performance for flows that involve rotation, boundary layers under strong adverse pressure gradient, and recirculation.

To determine the turbulent viscosity, realisable $k-\varepsilon$ turbulence model solves the transport equations of turbulent kinetic energy k and it's dissipation rate ε. The turbulent viscosity is calculated from

$$\mu_t = \rho C_\mu \frac{k^2}{\varepsilon}$$

4.2 SETTING INITIAL CONDITIONS FOR THE DISCRETE PHASE MODELLING

In this section, we will begin with the setup for the approach to the Lagrangian discrete phase model by defining the parameter required for the simulation. In the previous chapter, we've discussed that the fluid is treated as a continuum by solving Navier-Stokes equations, while the dispersed phase is solved by tracking a large number of a particle through the calculated flow field. We will neglect the exchange of momentum, mass, and energy with the fluid since it not relevant to the objective of this work.

4.2.1 Injection type

ANSYS Fluent in Discrete Phase Models provides 11 types of injections depending on the type of fluid problem engineers trying to solve. In the previous section, we defined our inlet and outlet for

water flow. There are two ways in which particle can be injected into the fish tank; inlet current water or top surface. Since the inlet of water is coming from underneath the tank, from a practical point of view, it would not possible to inject the particle from this point. Therefore, feeding pellets will be distributed from the top of the tank and any residual of this particle will fall under the bottom of tank before washed away by the outlet current. *The surface injection* will be the type of injection used for the first defined parameter. The feed (particle) is irregular organic material with an irregular shape that is difficult to characterize. For our assumptions, it has the same correlation given.

The type of particle use for this simulation will be *inert particle* (having no inherent ability to move or to resist motion).

4.2.2 Material

The material (not for massless particle) indicates the material for the particle. In the third chapter, we have produced the particle diameter and density based on their settling rate. We will create manually the particle properties based on the experimental result. In addition, the particle we are dealing has an irregular shape which means we have to set the physical model to the non-spherical model. The shape factor (sphericity) corresponds to the drag law coefficient and it is 0.874. It also important to note that water will be our medium under the category of material. Table (8) summarized the conditions for our defined injection.

Table 8. Parameter condition for Discrete Phase Module

Fluid			Inert Particle			Physical Models
Type	Density	Viscosity	Type	Diameter	Effective Density	Shape factor
Water	998.2	$1.004e^{-4}$	TM0	0.0035	1054.4	0.874
			TM75	0.0034	1072.9	0.874

4.2.3 Coupling

As mention in the earlier chapter, there are three different approach to analyze particle trajectories in some control volume over a medium. The simulation performed in this work is based on the one-way coupling. For one-way coupling calculations, only the fluid pressure acting at the structure is transferred to the structure solver. Initially, the fluid field is solved until convergence criteria are reached usually around 10^{-4} to 10^{-3}. The calculated forces at the structure boundaries are then transferred to the structure side. Next, the structure side is calculated until the convergence criterion is reached. Then, the fluid flow for the next time step is calculated to convergence. The solution is finished when the maximum number of time steps is reached. A benift to this approach is that

computational time is significantly reduced and that deformation of the fluid mesh does not included in the calculation, which provides a mesh of constant quality.

CHAPTER V CFD-DPM SIMULATION

5.1 CFD PROBLEM SETUP

5.1.1 Solver

Pressure based solver was selected for the simulation. The objective of this simulation is to produce a fully-developed flow profile in the tank. The simulation was performed as steady state. The discharged velocity are 0.08 m/s, 0.04 m/s, 0.8 m/s, 0.4 m/s which flow through inlet pipe having a diameter of 5 cm, thus turbulent model must be used for the case of the flow field in the tank (Reynolds number greater than 2300). We will set number of iteration up to 3000 for every change made in the inflow of material (water) until they converged. The continuity equation ideally should get below order 10^{-3} to get a converged solution.

We created surface, medium and bottom plane in order to obtain the velocity profile, so that we could check the symmetricity with respect to Y-Z plane (previous work by Ipek, 2019, was not very successful with this).

5.1.2 Boundary conditions

- Inlet velocity – different inlet velocities are used as state previously. In addition, the turbulence intensity ($\iota = v'/v$) and turbulence length scale $\left(\ell = C_\mu \frac{k^{3/2}}{\varepsilon}\right)$ were required to defined the inlet boundary conditions. Because the flow was discharged through inlet pipe of 5 cm, the turbulent intensity and length scale at the inlet were considered to be in order of 5%.
- Interior – solid(interior)
- Outlet – pressure (outlet)
- Surface – symmetry
- Wall – solid (stationary)

5.2 RESULT AND COMPARISON OF VELOCITY MAGNITUDE

Before the evaluation of velocity is deployed, it is important to consider the positions on which we can analyze the overall performance of the developed velocity for each different inlet parameter selected. The points are in accordance with the work of (Ipek, 2019). The aim is to produce a uniform field pattern. As suggested, a uniform velocity field was found to increase the rate of suspended particle deposition (Shahrokhi, Rostami, Said , Yazdi, & Syafalni , 2012).

Figure 9 (a)-(d) show the contour velocity magnitude at different operating conditions. Each contour plot has the scale according to the maximum velocity of that conditions. Referring to figure 9 (a), the calculation converged around 225 iteration which is a relatively low number. When the inlet velocity increases 10 times greater, the number iteration it required for simulation to converged increases dramatically. At one point, the continuity level never reached our ideal convergence criteria. For example, with an inlet velocity of 0.4 m/s, it required around 6000 iterations. Nevertheless, simulation result is still viable for comparison with the previous case. In addition, it can be seen clearly at each different inlet conditions, the flow intensity tends to deviate from the center as the flow rate increases. On a general note, the flow near the wall boundaries approaches to zero which means solid particle (pellet) will spread out across the surface before accelerating down when reaching near the wall. Although the flow velocities are relatively small, the vertical flow field will prevent the particle from sinking through the bottom of the tank rapidly.

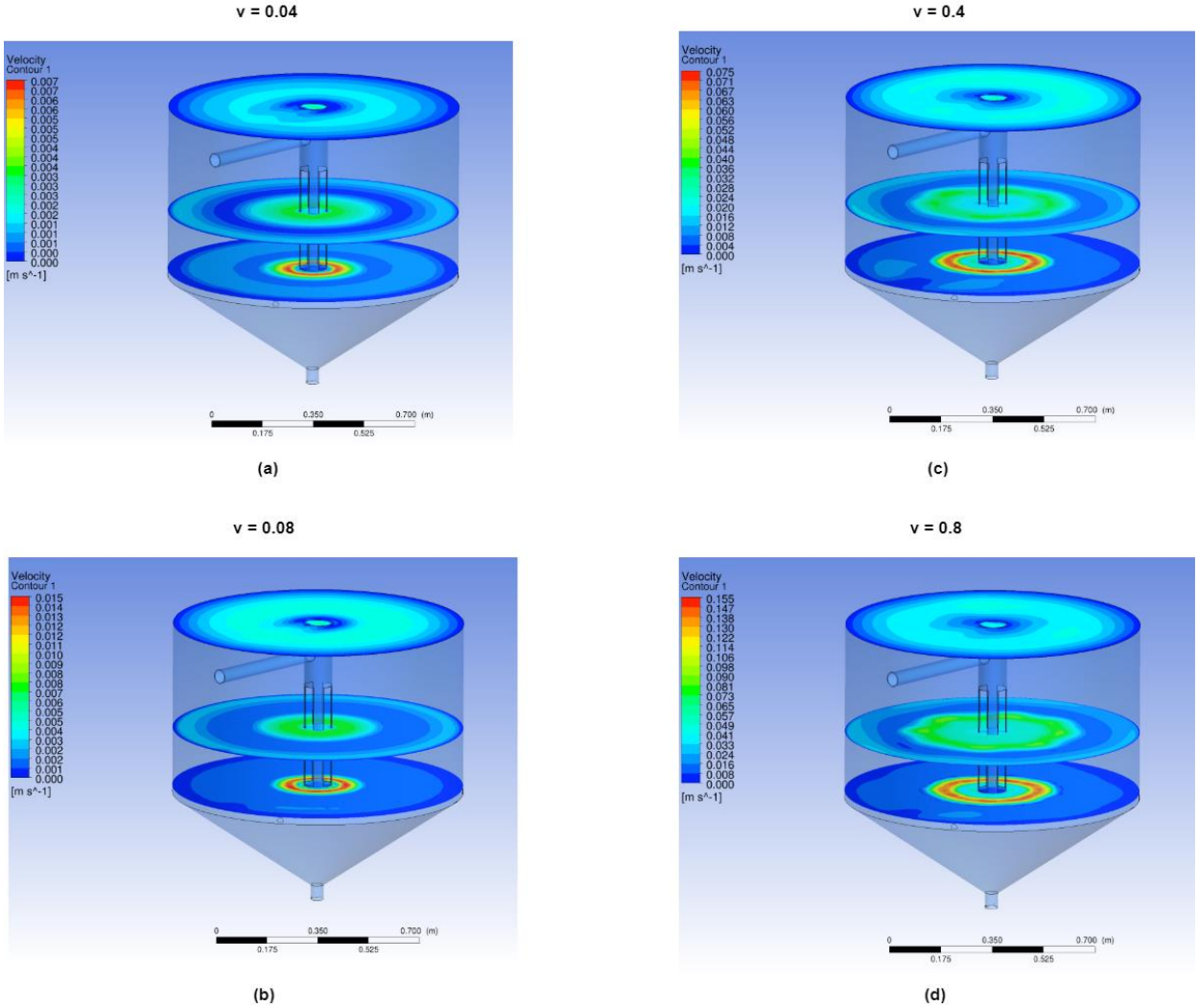

Figure 9. Contour of vertical velocity components in three horizontal planes in the fish tank at different inlet velocity operating parameter in m/s.

5.3 PARTICLE MOTION

Although the volume fraction of solids in the tank is very small compared to the size of the tank itself, the particle adversely impacts the water quality and hence the welfare and performance of the fish (Rosenthal, 1982; Braaten, 1986). Uneaten feed pellets and fish feces, if left untreated will be decomposed or hydrolyzed by microorganisms which reduce dissolved oxygen in the water and increases concentrations of CO_2, NH_3, and other mineral nutrients. Thus, the uneaten feed particle should be removed before it degraded into a fine particle. To facilitate an effective self-cleaning action, optimal flow conditions and structural design are necessary.

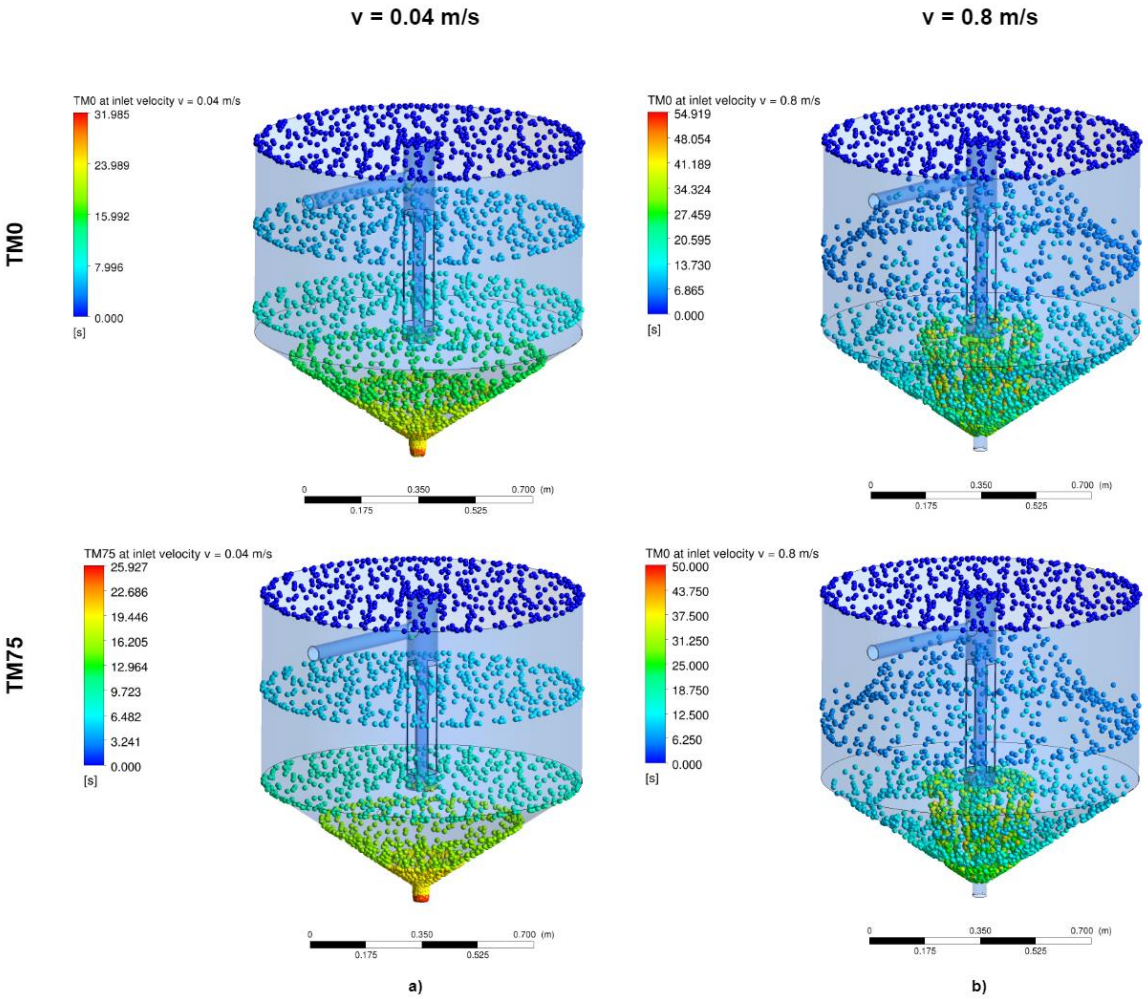

Figure 10. Feed pellet dispersion in fish tank injected from the free surface.

In order to evaluate the particle motion in the selected design, two type of particles (TM0 and TM75) were used to investigate the motion of solids in the tank. The density plays a major role on the settling rate of feed pellet. The density was determined experimentally (see chapter 3). Also, the settling velocity of the particle varies with the size of the particles.

In order to evaluate the particle motion in the selected design, two types of particles (TM0 and TM75) were used to investigate the motion of solids in the tank. The density plays a major role in

the settling rate of the feed pellet. The density was determined experimentally (see chapter 3). Also, the settling velocity of the particle varies with the size of the particles. In order to track the particle through the longest traveling distance, the particles were injected at the water surface. For the sake of simplicity, the number of particles tracked was limited to 500 to fully develop the Eulerian flow field. It was also assumed there were no collisions among the particles. A standard wall interaction with a coefficient of 0.5 for the particle was used in the solution process.

Figure 11 (a) and (b) show the resulting distribution of particles in the fish tank for the selected inlet configuration injected from the free surface. Two inlet velocities were studied from lowest to highest respectively. As soon as the particle enters the fluid domain, the particle accelerated downwards instantly, although the time for settling is higher than the average flow of the fluid domain, except for the inlet and outlet flow. Figure 11 (b), the inlet flow selected is the highest and it can be seen region near the outlet, the particle tends to fall slower compared to the region near-wall boundaries. This is explained in the previous section, the fluid flow approach zero which means they tend to accelerate the feed pellet faster on their way down the bottom. One logical reason is that flow is not sufficient enough to return them to the surface. Figure 11 (a) and (b) show the pellet having the same effective density as fluid (water). It can be seen clearly that the settling rate tends to increase significantly.

In chapter 3, expansion rate of pellet during settling can be considered but the simulation result is shows that the longest settling rate was around 500 seconds with the highest flow field domain. In the experiment, for pellet to increase 30% of its original size, it required almost 15 minutes of soaking until changes are noticed. This also reduce its density but in order to produce the same effect, the tank design i.e. its height must increase which require more investment and time.

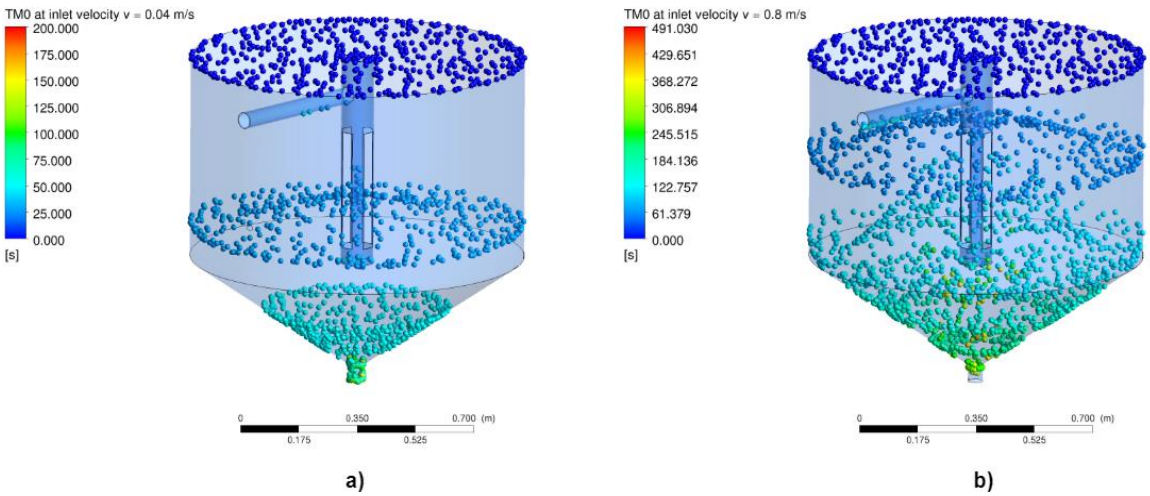

Figure 11. Fish pellet TM0 injected from surface with the same effective density as fluid (water) at different water inlet parameter

CHAPTER VI CONCLUSION

This work presents the development of CFD models of containment aquaculture. There is a lack of scientific information for the further development of innovative solutions in the field of hydrodynamics in aquaculture systems. Using CFD, this study has further developed new designs to improve flow patterns. The three following aspects are worth noting.

Sedimentation analysis was employed to determine the properties of the pellet (effective density) falling through a fluid at given conditions. Although the experiment was enough to get necessary properties for the simulation model, the measurement can be improved if we manage to use better and more reliable equipment. However, the error is still relatively small and can be cross-referenced with other research available.

Ipek (2019) studied the flow characterization of different fish tank volumes (2000, 500, 400l) using CFD simulation. The present work further investigates using different inlet parameter for one tank volume (500l). Having created the fluid flow domain, we found out that $k-\omega$ SST turbulence model does not converge with higher inlet velocities. Figure 12 can be seen that as flow field are not fully developed and are not symmetric. Hence, it was not suitable for further analysis since the continuity equation never reaches ideal convergence criteria. That is why $k-\varepsilon$ turbulence model was used in this case.

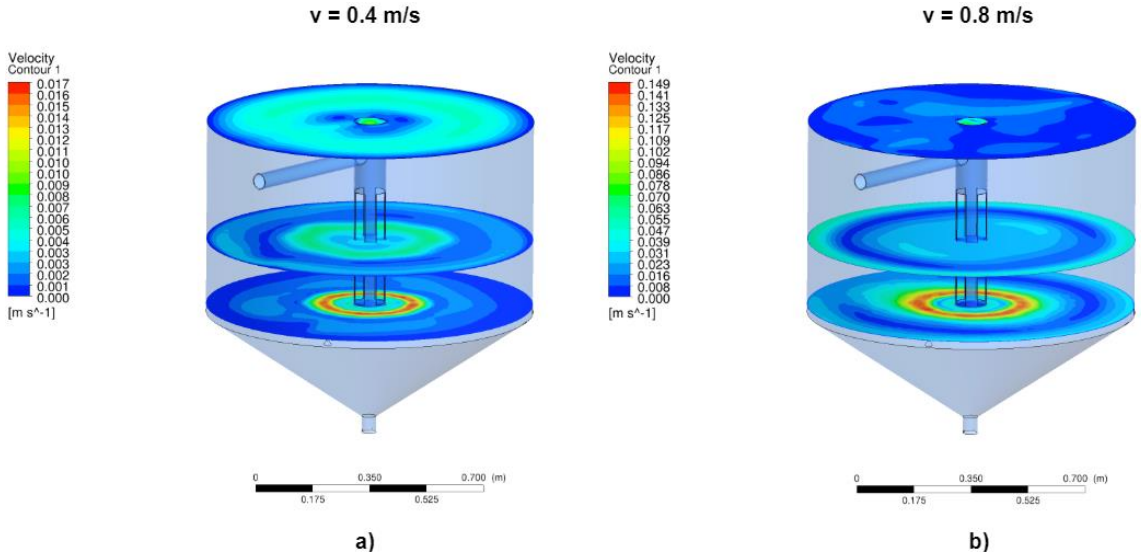

Figure 12. Contour of vertical velocity components with $k-\omega$ *SST* turbulence model.

The particle flow distribution of feed pellets was performed after creating a suitable flow field domain. The simple particle-tracking model used in the present study did not consider collisions between particles and their impact on the flow field. This approach substantially reduces simulations times.

From DPM simulation, we analyzed the motion of the particle as they settle down the tank. The motion of the feed pellet was well captured in this study. Particle settling occurs along the flow length under the influence of kinetic energy of flow and the gravity force. Figure 10 (a) and (b) shows with an inlet velocity of 10 times larger than commonly used (0.04 m/s, Like et al., 2015), the two types of particle with measured densities will fall to the bottom quickly (less than 60 seconds). Therefore, if we wanted to prevent fast settling of pellets and their accumulation at the bottom, the effective density should be quite close to the density of water. The methodology presented in this work could be used to find out optimal properties of feed pellets as well as other operational or geometrical parameters of a given fish tank.

In the field of aquaculture, we know the present work dealing with pellet and correct setting of the model in CFD solver is still very recent. The turbulence model such Reynolds stress model (RSM) can be used with fine mesh to generate better field flow while the mechanical and physical properties of the fish pellet can be better established with the further research as it gives a better representation of the residence time when tracking particle flowing in the fluid domain. Regardless, such a CFD model can be useful for researchers and aquaculturists which concern about fish farming.

REFERENCES

Alliance, G. A. (2019, March 27). Retrieved from www.aquaculturealliance.org: https://www.aquaculturealliance.org/blog/what-is-aquaculture-why-do-we-need-it/

ANSYS, Inc. (2012). *ANSYS Fluent User's Guide*. Retrieved from https://www.afs.enea.it/project/neptunius/docs/fluent/html/ug/node1.htm

Braaten, B. P. (1986). Risks from self-pollution in aquaculture: evaluation and consequences. *Aquaculture, 86*, 139-165.

Burley, R. K. (1985). Flow distribution studies in fish rearing tank. . Part 2. Analysis of hydraulic performance of 1 m square tank. *Aquaculture Engineering* , 113-134.

Celik, I. G. (2008). Procedure for estimation and reporting of uncertainty due to discretization in CFD. *ASME J. Fluids Eng, 7*, 078001-4.

Chen et. al., Y. S. (1999). Settling rate characteristics and nutrient content of the faeces of Atlantic salmon, Salmo salar L., and the implications for modelling of solid waste dispersion. *Aquaculture Research, 30*, 395-398.

Clift, R., Grace, J. R., & Weber, M. E. (2005). Bubbles, Drops, and Particles.

Crowe, C. T., Schwarzkopf, J. D., Sommerfeld , D., & Tsuji, Y. (2011). *Multiphase Flows with Droplets*. CRC Press.

Elghobashi, S. (1994). On predicting particle-laden turbulent flows. *Applied Scientific Research, 52*, 309-329.

H. Wadell, J. F. (1934).

Haider , A., & Levenspeil , O. (1989). Drag Coefficient and Terminal Velocity of Spherical and. *Powder Technology, 58*, 63-70.

Hinze., J. O. (1975). *Turbulence.* New York: McGraw-Hill Publishing Co.

Ipek, M. (2019). *CFD analysis of flow in fish tank.* Prague, Czech Republic: Czech Technical University in Prague.

Isaacs, J. L., & Thodos , G. (1967). The free-settling of solid cylindrical particles in the turbulent regime. *The Canadian Journal of Chemical Engineering, 45*, 150-155.

Karabulut , H. A., & Yandi, I. (2011). A Mercury Displacement Method to Measure Fish Feed Density. *Animal and Veterinanry Advances, 12*, 1516-1522.

Khater, E.-S. G., & Ali, A. H. (2014). Physical and Mechanical Properties of Fish Feed Pellets. *Food Processing & Technology, 5*(10). Retrieved from http://dx.doi.org/10.4172/2157-7110.1000378

Kothari , A. P., & Anderson , J. D. (1985). Flows Over Low Reynolds Number Airfoils - Compressible Navier-Stokes Numerical Solution. *Aerospace Sciences Meeting*, (pp. 14-17). Reno.

KWAŚNIEWSKI, L. (2013, May). Application of grid convergence index in FE computation. *BULLETIN OF THE POLISH ACADEMY OF SCIENCES, 61*. Retrieved from CFD Application in Process Engineering.

Lai, A. C., & Chen, F. Z. (2007). Comparison of a new Eulerian model with a modified Lagrangian approach for particle distribution and deposition indoors. *Atmospheric Environment, 41*, 5249-5256,.

Lika, K., & M. M. Pavlidis, N. M. (2015). Do experimental units of different scale affect the biological. *Journal of Fish Biology, 86*, 1271-1285.

Morsi, S. a. (1972). An investigation of particle trajectories in two-phase flow. *Journal of Fluid Mechanics, 55*, 193-208.

NASA, N. (n.d.). *Examining Spatial (Grid) Convergence*. (Alliance Vertification and Validation) Retrieved from http://www.grc.nasa.gov/WWW/wind/valid/tutorial/spatconv.html.

Roache, P. (1998). *Fundamentals of Computational Fluid Dynamics.* Albuquerque, New Mexico,: Hermosa Publisher .

Rosenthal, H. H.-J. (1982). Water management in circular tanks of a commercial intensive culture unit and its effects on water quality and fish condition. *ICES Statutory meeting, C.M.*, 13.

Shahrokhi, M., Rostami, F., Said , M. M., Yazdi, S. S., & Syafalni , S. (2012). The effect of number of baffles on the improvement efficiency of primary sedimentation tanks. *Applied Mathematical Modelling*, 3725-3735.

Stokes, G. G. (1851). n the Effect of the Internal Friction of Fluids on the Motion of pendulums. *9*.

Tvinnereim, K. (1988). Design of water inlets for closed fish farms. *Aquaculture Engineering Technologies for the Future, 66*, 241-249.

Wang, L. P., & Stock, D. E. (1993). Dispersion of Heavy Particles by Turbulent Motion. *Journal of Atmospheric Science*(50), 1897-1913.

Watten, B. J., & Beck , L. T. (1987). Comparative hydraulics of rectangular cross-flow rearing unit. *Aquaculutre Engineering* , 127-140.

Watten, B. J., & Johnson , R. P. (1990). Comparative hydraulics and rearing trial performance of a production scale cross-flow rearing unit. *Aquaculture Engineering*, 245-266.

White, F. M. (1974). *Viscous fluid flow.* New York: McGraw-Hill.

Wojnar L., &. K. (2000). *Practical Guide to Image Analysis.* United State: ASM Internaltional.